Optimal Focal-Plane Restoration

Stephen E. Reichenbach Stephen K. Park

Computer Science Department
College of William and Mary
Williamsburg, Virginia

Abstract

Image restoration can be implemented efficiently by calculating the convolution of the digital image and a small kernel during image acquisition. Processing the image in the focal-plane in this way requires less computation than traditional Fourier-transform-based techniques such as the Wiener filter and constrained least-squares filter. In this paper, the values of the convolution kernel that yield the restoration with minimum expected mean-square error are determined using a frequency analysis of the end-to-end imaging system. This development accounts for constraints on the size and shape of the spatial kernel and all the components of the imaging system. Simulation results indicate the technique is effective and efficient.

1 Introduction

The Wiener filter is probably the best known and most widely used restoration tool. Given a few assumptions and some knowledge of the system, the Wiener filter minimizes the expected mean-square-error (MSE) of the restoration. While MSE is by no means a perfect yardstick for restoration quality, it is a useful measure and leads to an optimal filter. In many applications, such as those requiring television-rate processing (30 images per second), the most serious drawback of the Wiener filter is its high computational cost. Small spatial kernels can be applied with much less computation. This paper describes the design of small restoration kernels that, within the spatial constraints, minimize restoration MSE.

2 End-to-End Analysis and Wiener Restoration

Traditionally, Wiener restoration has been based on a model of the imaging process with two components: the linear, shift-invariant point-spread function (PSF) of the image acquisition device and additive, signal-independent noise. This model ignores the significant impact of sampling and display reconstruction on image quality. A recent paper[1] presented a derivation of the Wiener filter that is based on a more accurate model of the end-to-end imaging process. This model is illustrated in Figure 1.

The end-to-end process is described equivalently by equations in either the spatial domain or frequency domain. The displayed (or resulting) image r is

$$r(x) = \frac{1}{N}\sum_{n'}\frac{1}{N}\sum_{n}\left(\frac{1}{N}\int_{-\infty}^{\infty} s(n-x')h(x')dx'\text{Ш}(n)+e[n]\right) f[n'-n]d(x-n') \qquad (1)$$

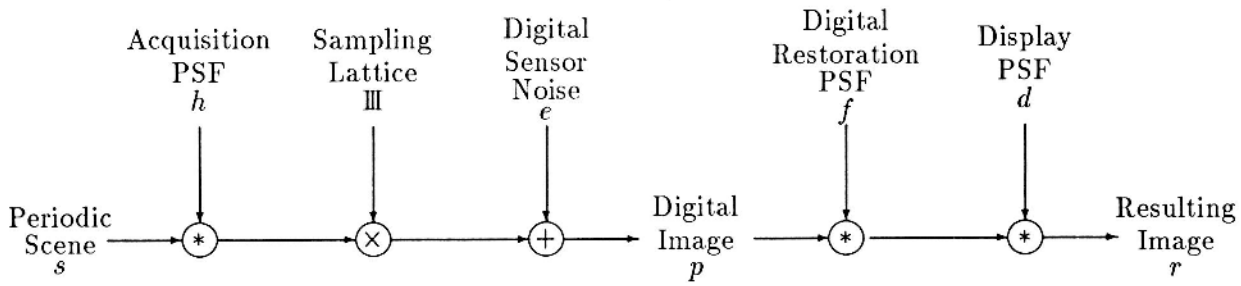

Figure 1: End-to-End Imaging and Spatial Restoration Model

Assuming the scene s is periodic, the equivalent frequency domain expression for the spectrum of the result $\hat{r}$ is

$$\hat{r}[\nu] = \left(\sum_{\nu'=-\infty}^{\infty} \hat{s}[\nu']\hat{h}[\nu']\hat{\text{Ш}}[\nu - \nu'] + \hat{e}[\nu] \right) \hat{f}[\nu]\hat{d}[\nu] \tag{2}$$

where the notation $\hat{r}[\nu]$ indicates the spatial frequency ν/N, ν cycles per N spatial units, of the Fourier transform of the image r.

The Wiener filter minimizes the expected mean-square difference between the scene s and the resulting image r:

$$\begin{aligned} S^2 &= E\left\{ \frac{1}{N} \int_0^N |s(x) - r(x)|^2 \, dx \right\} \\ &= E\left\{ \sum_{\nu=-\infty}^{\infty} |\hat{s}[\nu] - \hat{r}[\nu]|^2 \right\} \end{aligned} \tag{3}$$

If the scene s and noise e are uncorrelated, stationary processes with power spectra Φ_s and Φ_e respectively, the expected mean-square restoration error can be rewritten in a form that is suitable for minimization:

$$\begin{aligned} S^2 = \sum_{\nu=-\infty}^{\infty} N \Bigg(& \sum_{\nu'=-\infty}^{\infty} \Phi_s[\nu']\hat{\text{Ш}}[\nu - \nu'] \\ & - \sum_{\nu'=-\infty}^{\infty} \Phi_s[\nu']\hat{h}^*[\nu']\hat{d}^*[\nu']\hat{\text{Ш}}[\nu - \nu']\hat{f}^*[\nu] - \sum_{\nu'=-\infty}^{\infty} \Phi_s[\nu']\hat{h}[\nu']\hat{d}[\nu']\hat{\text{Ш}}[\nu - \nu']\hat{f}[\nu] \\ & + \left(\sum_{\nu'=-\infty}^{\infty} \Phi_s[\nu'] \left|\hat{h}[\nu']\right|^2 \hat{\text{Ш}}[\nu - \nu'] + \Phi_e[\nu] \right) \left(\sum_{\nu'=-\infty}^{\infty} \left|\hat{d}[\nu']\right|^2 \hat{\text{Ш}}[\nu - \nu'] \left|\hat{f}[\nu]\right|^2 \right) \Bigg) \end{aligned} \tag{4}$$

Minimizing the mean-square error with respect to the filter transfer function values $\hat{f}[\nu]$ leads to the

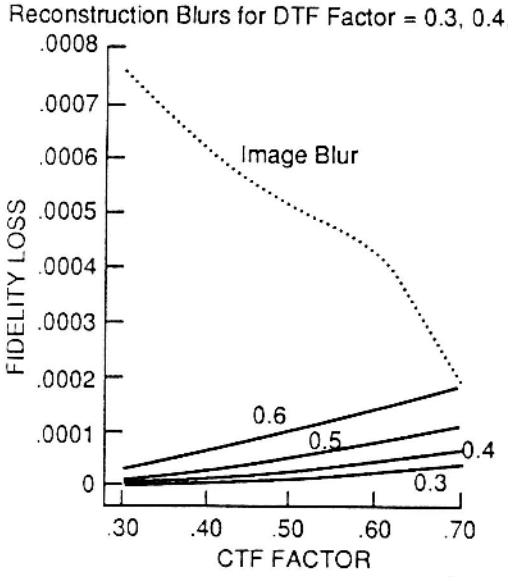

Figure 12: Reconstruction Blur vs CTF FACTOR (Cat)
(for DTF FACTOR = 0.3 to 0.6)

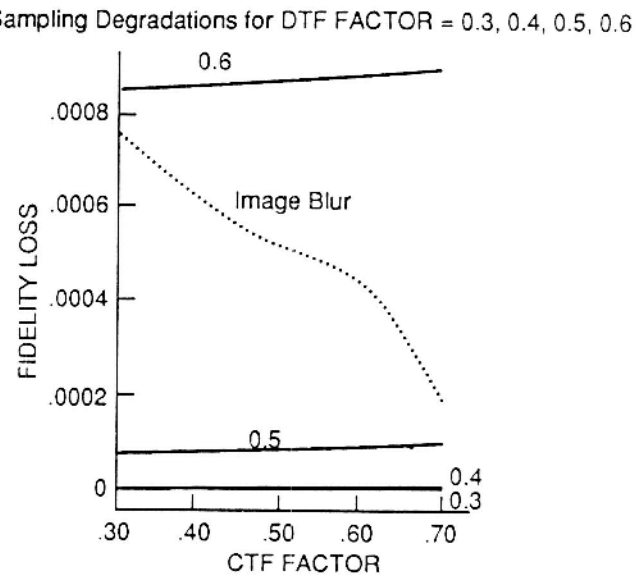

Figure 13: Sampling Blur vs CTF FACTOR (Cat)
(for DTF FACTOR = 0.3 to 0.6)

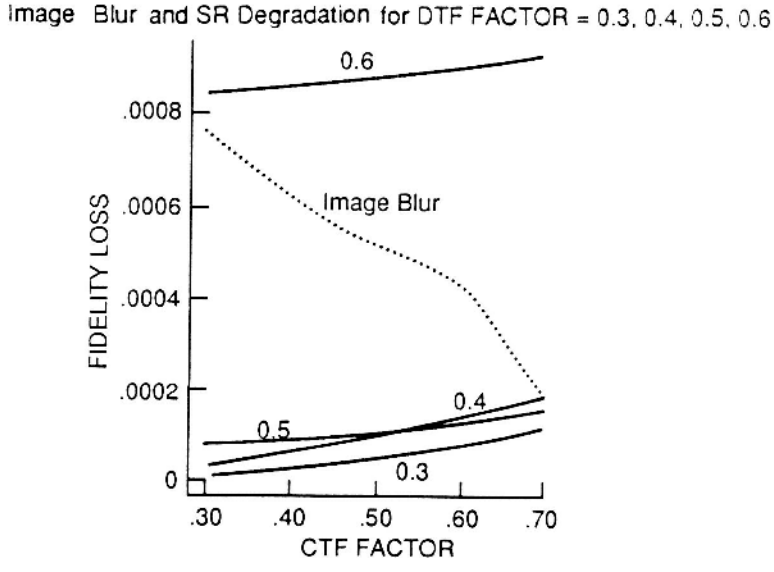

Figure 14: Image and SR Blur vs CTF FACTOR (Cat)
(for DTF FACTOR = 0.3 to 0.6)

Fig 15 : Original Dollar Image with no image and SR degradations.

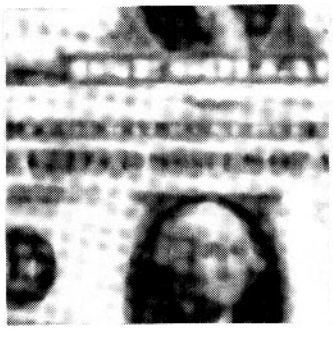

Fig 16 : Reconstructed Scene with CTF FACTOR=0.3 and DTF FACTOR=0.3

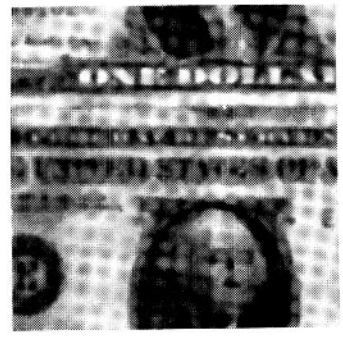

Fig 17 : Reconstructed Scene with CTF FACTOR=0.3 and DTF FACTOR=0.7

definition of the optimal filter:

$$\hat{f}[\nu] = \frac{\sum_{\nu'=-\infty}^{\infty} \Phi_s[\nu']\hat{h}^*[\nu']\hat{d}^*[\nu']\hat{\mathbb{III}}[\nu-\nu']}{\left(\sum_{\nu'=-\infty}^{\infty} \Phi_s[\nu']\left|\hat{h}[\nu']\right|^2 \hat{\mathbb{III}}[\nu-\nu'] + \Phi_e[\nu]\right)\left(\sum_{\nu'=-\infty}^{\infty} \left|\hat{d}[\nu']\right|^2 \hat{\mathbb{III}}[\nu-\nu']\right)} \tag{5}$$

This is the optimal digital filter given in Equation 26 of [1].

The mathematics of the following section is simplified by rewriting the expression for mean-square error in Equation 4 as

$$S^2 = \sum_{\nu=-\infty}^{\infty} N\left(\hat{c}[\nu] - \hat{b}[\nu]\hat{f}^*[\nu] - \hat{b}^*[\nu]\hat{f}[\nu] + \hat{a}[\nu]\left|\hat{f}[\nu]\right|^2\right) \tag{6}$$

where

$$\hat{a}[\nu] = \left(\sum_{\nu'=-\infty}^{\infty} \Phi_s[\nu']\left|\hat{h}[\nu']\right|^2 \hat{\mathbb{III}}[\nu-\nu'] + \Phi_e[\nu]\right)\left(\sum_{\nu'=-\infty}^{\infty} \left|\hat{d}[\nu']\right|^2 \hat{\mathbb{III}}[\nu-\nu']\right) \tag{7}$$

$$\hat{b}[\nu] = \sum_{\nu'=-\infty}^{\infty} \Phi_s[\nu']\hat{h}^*[\nu']\hat{d}^*[\nu']\hat{\mathbb{III}}[\nu-\nu'] \tag{8}$$

$$\hat{c}[\nu] = \sum_{\nu'=-\infty}^{\infty} \Phi_s[\nu']\hat{\mathbb{III}}[\nu-\nu'] \tag{9}$$

Then, the optimal filter transfer function $\hat{f}$ given by Equation 5 is written:

$$\hat{f}[\nu] = \frac{\hat{b}[\nu]}{\hat{a}[\nu]} \tag{10}$$

3 Imposing Spatial Constraints

In the derivation of the previous section, the Wiener filter is determined by an equation in the frequency domain:

$$\hat{a}[\nu]\hat{f}[\nu] = \hat{b}[\nu] \tag{11}$$

The spatial equivalent of this frequency domain product is the spatial convolution:

$$\frac{1}{N}\sum_{n'} a[n-n']f[n'] = b[n] \tag{12}$$

where

$$a[n] = \sum_{\nu} \hat{a}[\nu]W_N^{\nu n} \tag{13}$$

$$b[n] = \sum_{\nu} \hat{b}[\nu]W_N^{\nu n} \tag{14}$$

This convolution is equivalently expressed as a linear system of N equations in N variables (the spatial filter values). The system of equations can be expressed in matrix form:

$$\mathbf{Af} = \mathbf{b} \tag{15}$$

where the $N \times N$ coefficient matrix $\mathbf{A}$ is

$$\mathbf{A}[n', n''] = \frac{1}{N} a[n' - n''] \tag{16}$$

the $N \times 1$ result matrix $\mathbf{b}$ is the array b defined in Equation 14, and $\mathbf{f}$ is the $N \times 1$ matrix of digital restoration PSF values to be determined.

In the system of equations for the Wiener filter, there are as many equations as pixels in the image. However, if the size of the spatial restoration kernel is constrained, the system of independent equations can only be as large as the number of nonzero elements in the spatial kernel. The spatially constrained kernel is designed by specifying the system of linear equations whose solution will minimize mean-square-error within the constraints.

The spatial constraint is expressed as a nonempty set of spatial locations, C, for which the restoration kernel can be nonzero. The elements that are not in the constraint set must be zero:

$$f[n] = 0 \quad \text{if} \quad n \notin C \subseteq \{0 \ldots N-1\} \tag{17}$$

If all of the points in the restoration kernel are allowed to be nonzero (i.e., $C = \{0 \ldots N-1\}$), then the optimal spatial kernel is the inverse transform of the Wiener filter (i.e., the solution of Equation 12 or 15).

The expression for MSE is defined in Equation 6 in terms of the transfer function of the optimal filter. Before this expression can be minimized with respect to the restoration kernel values, it must be expressed in terms of those elements. The filter transfer function expressed in terms of the spatially constrained kernel values is

$$\hat{f}[\nu] = \frac{1}{N} \sum_{n \in C} f[n] W_N^{-\nu n} \tag{18}$$

Substituting this expression into Equation 6, yields the MSE in terms of the constrained kernel values:

$$\begin{aligned}
S^2 &= \sum_{\nu} \left(\hat{c}[\nu] - \hat{b}[\nu] \left(\frac{1}{N} \sum_{n' \in C} f^*[n'] W_N^{\nu n'} \right) - \hat{b}^*[\nu] \left(\frac{1}{N} \sum_{n' \in C} f[n'] W_N^{-\nu n'} \right) \right. \\
&\qquad \left. + \hat{a}[\nu] \left| \frac{1}{N} \sum_{n' \in C} f[n'] W_N^{-\nu n'} \right|^2 \right) \\
&= \sum_{\nu} \hat{c}[\nu] - \frac{1}{N} \sum_{n' \in C} f^*[n'] \sum_{\nu} \hat{b}[\nu] W_N^{\nu n'} - \frac{1}{N} \sum_{n' \in C} f[n'] \sum_{\nu} \hat{b}[\nu] W_N^{-\nu n'} \\
&\quad + \frac{1}{N^2} \sum_{n' \in C} \sum_{n'' \in C} f^*[n'] f[n''] \sum_{\nu} \hat{a}[\nu] W_N^{\nu (n' - n'')} \\
&= \sum_{\nu} \hat{c}[\nu] - \frac{1}{N} \sum_{n' \in C} f^*[n'] b[n'] - \frac{1}{N} \sum_{n' \in C} f[n'] b^*[n'] \\
&\quad + \frac{1}{N^2} \sum_{n' \in C} \sum_{n'' \in C} f^*[n'] f[n''] a[n' - n'']
\end{aligned} \tag{19}$$

Minimizing with respect to the restoration kernel elements yields

$$\frac{1}{N}\sum_{n'\in C} f[n']a[n-n'] \;=\; b[n] \qquad n \in C \tag{20}$$

This is an equation with a number of unknowns equal to the number of non-zero kernel values—$|C|$. There are $|C|$ equations (differentiating with respect to each of the constrained kernel elements) in $|C|$ unknowns (the $|C|$ kernel values). This system of equations can be written as the matrix equation:

$$\mathbf{A}_C\mathbf{f}_C \;=\; \mathbf{b}_C \tag{21}$$

where $\mathbf{A}_C$ is the $|C| \times |C|$ coefficient matrix, $\mathbf{f}_C$ is the $|C| \times 1$ matrix of kernel values, and $\mathbf{b}_C$ is the $|C| \times 1$ result matrix.

The output matrix $\mathbf{b}_C$ of Equation 21 for the constrained filter is a submatrix of the corresponding matrix $\mathbf{b}$ of Equation 15 for the Wiener (unconstrained) filter. The elements of the matrix $\mathbf{b}_C$ are the elements of $\mathbf{b}$ that are in the constraint set C. Similarly, $\mathbf{A}_C$ is a principal submatrix [2] of the coefficient matrix $\mathbf{A}$ consisting only of the rows and columns of $\mathbf{A}$ named in the constraint set C.

4 Simulation Results

This section presents restoration results for artificial scenes degraded by simulated imaging devices (as described in [3]). The problem design included two variables: the width of the acquisition transfer function and the noise level. Three cases for each variable were considered, producing a total of nine experimental restoration problems. Each of the nine problems was restored with kernels constrained to a number of sizes. Then, the accuracy of the constrained restorations was compared to the accuracy of the unrestored display and Wiener restoration.

One-dimensional Fourier scenes were generated by specifying the spectral magnitude of a finite Fourier series and randomizing phase. The scene spectral magnitude $\hat{s}_\rho$ was set to

$$\hat{s}_\rho[\nu] \;=\; \begin{cases} K\exp\left(-\left(|\nu|/\alpha_s\right)^{\beta_s}\right) & \text{if } 0 < |\nu| < 2N \\ 0 & \text{otherwise} \end{cases} \tag{22}$$

with $\alpha_s = N/16$ and $\beta_s = 0.75$. Because the spectral magnitude is zero at the origin ($\hat{s}_\rho[0] = 0$), the resulting ensemble of scenes is zero-mean. The constant K was defined as 0.0704946 so that the scenes had unit root-mean-square RMS energy.

The model of the acquisition device transfer functions was suggested by Johnson[4]:

$$\hat{h}_\rho[\nu] \;=\; \exp\left(-\left(|\nu|/\alpha_h\right)^{\beta_h}\right) \tag{23}$$

All three of the transfer functions in this section are bell curves ($\beta_h = 2$).

- With $\alpha_h = 0.75$, the transfer function roll off is mostly above the Nyquist limit. This function attenuates frequency components within the Nyquist limit only slightly and will therefore cause little blurring. However, the transfer function significantly passes components above the Nyquist limit and is therefore vulnerable to aliasing.
- With $\alpha_h = 0.50$, the transfer function rolls off at a lower frequency and therefore causes somewhat more blurring, but is less vulnerable to aliasing.

- With $\alpha_h = 0.25$, the transfer function is nearly zero beyond the Nyquist limit. This function virtually eliminates aliasing, but the resulting images may be blurred substantially.

Three levels of zero-mean white noise were considered. Signal-to-noise ratio (SNR) is the ratio of RMS energy of the scene to RMS energy of the noise:

$$\text{SNR} \triangleq \sqrt{\frac{\sum_{\nu} |\hat{s}[\nu]|^2}{\sum_{\nu} |\hat{e}[\nu]|^2}} \tag{24}$$

For the low-noise images (high SNR), SNR=100. For the moderate-noise images, SNR=25. For the high-noise images (low SNR), SNR=5.

Real display devices are a significant component of the end-to-end imaging process but are not usually a source of much variability. Therefore, the simulated display function was not varied in these experiments—a single display model was used for all of the simulations. Schade[5] suggested a display model consisting of the sum of two Gaussian spots—the *nucleus*, a strongly-peaked central spot that contains most of the energy, and a broad *flare* spot around the nucleus. The composite display transfer function is

$$\hat{d}[\nu] = D_1 \exp\left(-\left(|\nu|/\alpha_1\right)^2\right) + D_2 \exp\left(-\left(|\nu|/\alpha_2\right)^2\right) \tag{25}$$

The parameters for the functions are taken from Schade's results: for the nucleus, $D_1 = 0.76$ and $\alpha_1 = 0.4301484$; for the flare, $D_2 = 0.24$ and $\alpha_2 = 0.0323814$. For practical reasons, the display transfer function is cut off at twice the sampling rate $\pm 2N$ (the same length as the Fourier series used to generate the artificial scenes). The effect of the truncation is insignificant.

Figure 2 illustrates the end-to-end imaging simulation for a representative scene. The top graph is the scene. Directly below it is the image created by applying the acquisition function with medium blur ($\alpha_h = 0.50$) to the scene. The third graph is the sampled image. Next is the sampled scene plus moderate noise (SNR = 25). The bottom graph of Figure 2 shows the unrestored display. Acquisition blurring, aliasing due to sampling, additive sensor noise, and display degradation are all present in the output of the system. The goal of restoration is to process the noisy digital image shown in the fourth graph so that when it is displayed, the output (the bottom line) is more like the input (the top line).

The spatial kernels were constrained to have zero value at all but an odd number of locations centered at the origin—the smallest kernel, with three elements, was allowed non-zero values only where $|n| \leq 1$; the next smallest, with five elements, was allowed non-zero values only where $|n| \leq 2$; and so on. The largest constrained kernel has $(N-1)$ elements; only the element at $n = N/2$ was constrained to 0. The next-largest optimal kernel (no elements constrained to 0) is the spatial kernel of the Wiener filter.

The optimal three-point and five-point kernels for the example of Figure 2 and the corresponding transfer functions are shown in Figure 3. The Wiener filter transfer function and part of the corresponding spatial kernel are also illustrated. Only the first few elements of the Wiener kernel are shown; the magnitude of the Wiener kernel elements beyond 6 pixels from the origin is less than $0.01N$. Clearly, the optimal small kernels are quite different than the kernels produced by a truncating the Wiener PSF. As can be seen by comparing the transfer functions, the optimal three-point kernel does a fair job of approximating the Wiener filter at low frequencies but amplifies high-frequency components where SNR is lower much more than does the Wiener filter. The transfer

function of the optimal five-point kernel more closely approximates the Wiener filter, but is still quite different.

Figure 4 shows the original scene, the unrestored output, the output with three-point restoration, the output with five-point restoration, and the output with Wiener restoration. Visual comparison is a subjective process, but it is clear that all of the restorations are more like the original scene than the unrestored output. It is more difficult to conclude from visual inspection which of the restorations is the best. Some of the features seem to be restored best by the three-point kernel; other features are best restored by the Wiener restoration.

Figure 5 presents numeric measures of restoration accuracy as a function of kernel size. Restoration accuracy is described by the RMS difference between the displayed image and the scene, relative to the RMS energy of the scene:

$$\text{Relative RMS Error} = \sqrt{\frac{\sum_{\nu} |\hat{s}[\nu] - \hat{r}[\nu]|^2}{\sum_{\nu} |\hat{s}[\nu]|^2}} \tag{26}$$

Each of the nine restoration problems was performed 32 times—that is, each execution used a different scene from the ensemble and different random noise. The plots show the relative RMS error averaged over all 32 executions. The standard deviations of the relative RMS error were so small that plotting them on these graphs proved impractical. The plots are shown only for kernels with 65 elements or fewer (radius 32). In all cases, only negligible improvement occurred beyond 19 elements (radius 9). (The kernel of the Wiener filter has 255 elements, a radius of 128.)

In many cases, the three-point and five-point kernels yielded results that are nearly as accurate as the Wiener filter. This is particularly true when there is little noise (e.g., SNR=100—the leftmost column). Small kernels are relatively less successful in low SNR situations (e.g., SNR=5—the rightmost column). In low SNR problems, the restoration kernel should suppress noise by local averaging, but small kernels are restricted in doing so by their size.

In the image with medium blur and medium noise ($\alpha_h = 0.50$ and SNR=25)—the middle graph of Figure 5—the average unrestored relative RMS error was 0.204613. The Wiener filter reduced this to 0.051149, a decrease of 0.1536464 or 75%. The three-point kernel resulted in an error of 0.091685, a decrease of 0.112928 or 55%. The three-point kernel (radius 1) achieved 73% of the improvement of the Wiener filter. The five-point kernel (radius 2) reduced the relative RMS error to 0.083614, a decrease of 0.120999 or 59%. This is 79% of the improvement of the Wiener filter. These small kernels achieve a large portion of the improvement of the Wiener filter with less computation.

5 Conclusion

Restoration implemented by convolution with a small kernel requires less processing than traditional Fourier-transform-based techniques such as the Wiener filter. Because convolution with a small kernel is a local operation, it is easily applied in parallel on all pixels in the focal-plane during image acquisition. The simulation results indicate that the optimal constrained restoration kernel effectively restores continuous, one-dimensional functions degraded by blurring, sampling, noise, and reconstruction—the types of degradations found in real imaging systems. Similar results were observed in simulations not presented in this paper using other one-dimensional scenes with different statistics. Two-dimensional simulations and actual restorations are in preparation.

References

[1] Carl L. Fales, Friedrich O. Huck, Judith A. McCormick, and Stephen K. Park. Wiener restoration of sampled image data: end-to-end analysis. *Journal of the Optical Society of America A*, 5(3):300–314, 1988.

[2] Roger A. Horn and Charles R. Johnson. *Matrix Analysis*. Cambridge University Press, New York, NY, 1985.

[3] Stephen E. Reichenbach and Stephen K. Park. Computer generated scenes and simulated imaging. In *Technical Digest of the Optical Society of America Annual Meeting*, page 170, 1988.

[4] C. B. Johnson. A method for characterizing electro-optical device modulation transfer functions. *Photographic Science and Engineering*, 14(6):413–415, 1970.

[5] Otto H. Schade, Sr. Image reproduction by a line raster process. In Lucien M. Biberman, editor, *Perception of Displayed Information*, chapter 6, pages 233–278, Plenum Press, New York, NY, 1973.

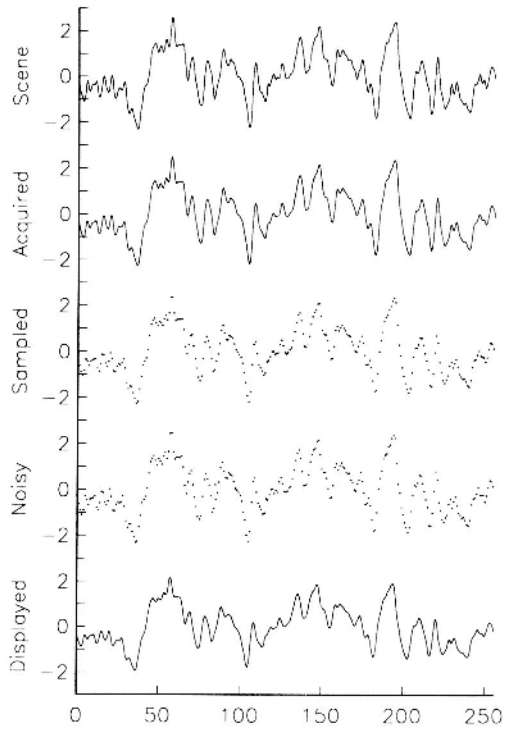

Figure 2: Simulated End-to-End Processing of a Representative Scene

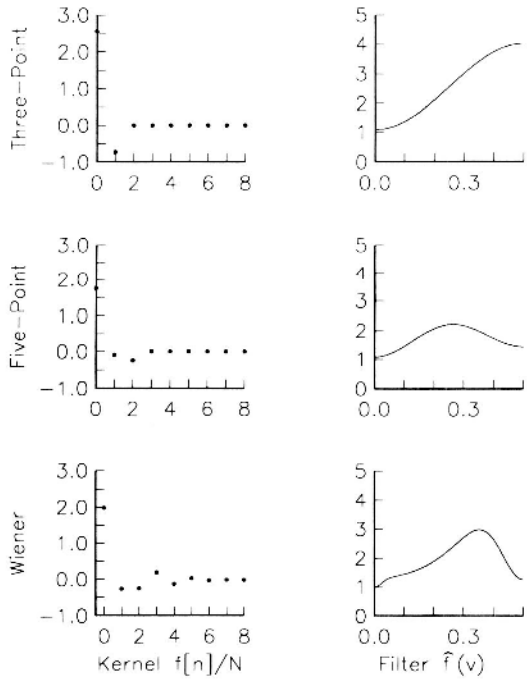

Figure 3: Restoration Functions

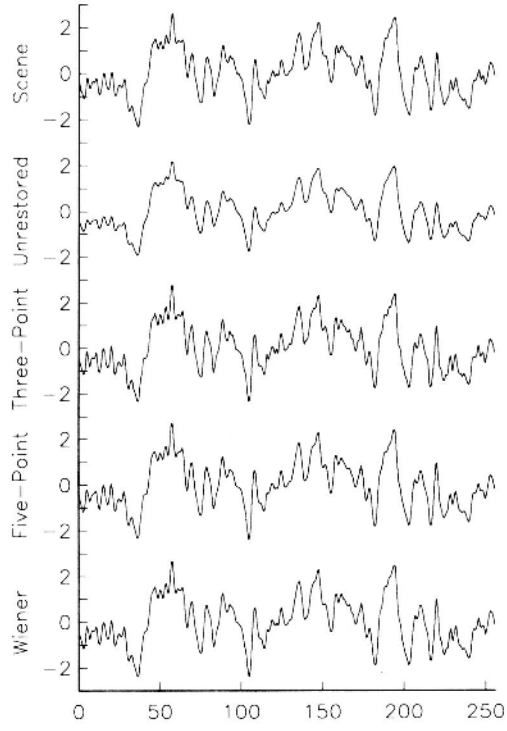

Figure 4: Representative Restoration Results

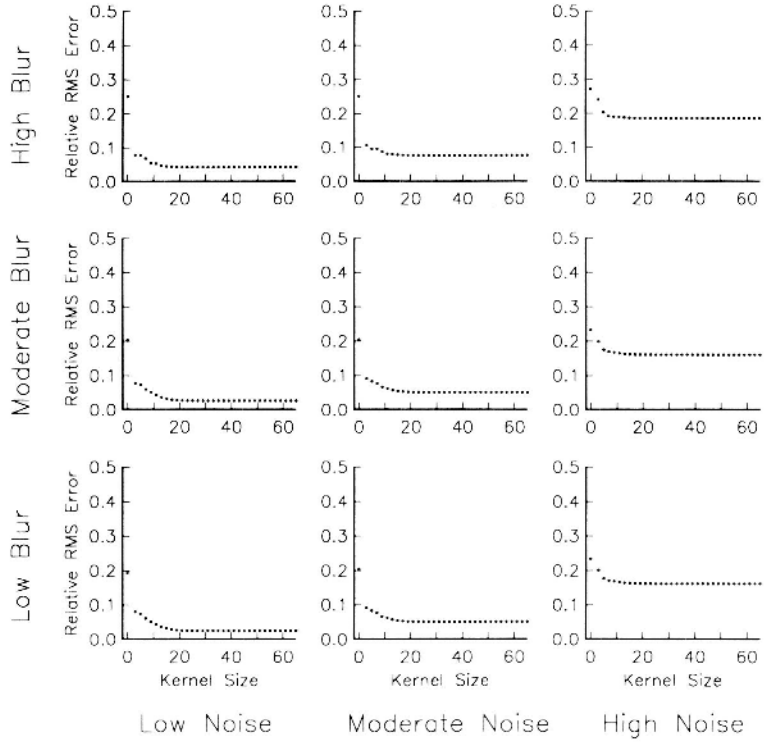

Figure 5: Relative Restoration Error